Carbohydrate Polymers 83 (2011) 1812–1820

Contents lists available at ScienceDirect

Carbohydrate Polymers

journal homepage: www.elsevier.com/locate/carbpol

Effect of side chain length on structure and thermomechanical properties of fully substituted cellulose fatty esters

Lucie Crépy[a,b,c], Valérie Miri[a,d,**], Nicolas Joly[a,b,c,*], Patrick Martin[a,b,c], Jean-Marc Lefebvre[a,d]

[a] Univ Lille Nord France, F-59000 Lille, France
[b] CNRS, UMR 8181, Unité de Catalyse et de Chimie du Solide, UCCS, F-59650 Villeneuve D'Ascq, France
[c] UArtois, IUT Béthune, UCCS, F-62408 Béthune, France
[d] Unité Matériaux Et Transformations, UMR CNRS 8207, Université Lille Nord de France, France

ARTICLE INFO

Article history:
Received 6 September 2010
Received in revised form 8 October 2010
Accepted 20 October 2010
Available online 27 October 2010

Keywords:
Cellulose fatty esters
Layered type structure
Side-chain crystallinity
Structure–properties relationships

ABSTRACT

A series of cellulose esters (CEs) with high degrees of substitution has been obtained by linking aliphatic acid chlorides (from C8 to C18) onto cellulose backbone, in a homogeneous LiCl/DMAc medium. These materials have been characterized by Fourier transformed infra red (FTIR) and nuclear magnetic resonance of proton (^{1}H NMR) spectroscopies, as well as differential scanning calorimetry (DSC), wide angle X-ray scattering (WAXS), dynamic mechanical analysis (DMA) and mechanical analyses. CEs organize in a layered type structure: cellulosic backbones are arranged in a plane, the flexible side chains being fully extended and perpendicular to the cellulosic backbone. When the fatty chain length exceeds 12 carbon atoms, a fraction of the alkyl chains crystallize into hexagonal packing. Regarding the mechanical behavior, the strain at break decreases significantly whereas no clear evolution of the yield stress is observed when the length of the lateral chain is increased.

1. Introduction

Cellulose esters (CEs) represent a class of commercially important thermoplastic polymers, with excellent fiber and filmogenic characteristics recognized for nearly a century (Edgar et al., 2001). They may be synthesized from natural and renewable raw materials. Moreover, these bio-based products can be obtained through a "green chemistry" approach, and offer interesting alternatives to petrochemical plastics, depending on their physical properties. Our preliminary studies (Crépy, Chaveriat, Banoub, Martin, & Joly, 2009; Joly et al., 2006) have demonstrated the possibility to obtain such thermoplastic materials by acylation of cellulose with fatty acids.

The effective use and high functionalization of cellulose have been investigated in recent years (Nagatani, Endo, Hirotsu, & Furukawa, 2005). In fact, native cellulose does not exhibit any thermoplastic behavior, due to strong inter- and intramolecular hydrogen bonding. Therefore, in common cellulosic plastics such as CEs (acetate, propionate, etc.) thermoplastic properties result from the esterification of cellulose (Edgar et al., 2001; Mohanty, Wibowo, Misra, & Drzal, 2003). CEs with a longer substituent (laurate for example) exhibit plasticized polymer behavior but without any addition of external plasticizer unlike the case of other biopolymers (Chauvelon et al., 2000; Thiebaud, Borredon, Baziard, & Senocq, 1997).

Numerous literature contributions concern cellulose chemical modifications, and particularly cellulose esters synthesis and properties (Edgar et al., 2001; Heinze & Liebert, 2001). The first studies of CEs thermal properties have shown that the melting point (T_m) increases slightly from C8 (octanoate) to C18 (stearate) (Malm, Mench, Kendall, & Hiatt, 1951; Morooka, Norimoto, Yamada, & Shiraishi, 1984). This increase is probably due to a diminution of substituent mobility related to the steric effects of the chain length substituent. With higher substituents, thermal transitions are less well-defined; glass transition (T_g) and T_m are closer to each other. Moreover, the longer the substituent is, the higher is the thermal stability (Chauvelon et al., 2000).

One of the most extensive study about CEs thermal properties (from C12 to C20 with a degree of substitution, DS, about 2.8–2.9) was carried out by Sealey et al. (Sealey, Samaranayake, Todd, & Glasser, 1996). Differential scanning calorimetry (DSC) analyses have shown two separate and distinct transitions for waxy CEs: a broad T_g near 100 °C, which increased linearly with substituent size, and a large T_m from −19 °C (C12) to 55 °C (C20). The increase of T_m values with the fatty chain length and the broadness of the corresponding peak were attributed respectively to the crystal size

* Corresponding author at: IUT de Béthune, 1230 rue de l'Université, BP819, F-62408 Béthune cedex, France. Tel.: +33 (0)3 21 63 23 20; fax: +33 (0)3 21 63 02 94.
** Corresponding author at: Unité Matériaux Et Transformations, UMR CNRS 8207, Université Lille Nord de France, Bât. C6, 59655 Villeneuve d'Ascq, France. Tel: +33 (0)3 20 33 64 16; fax: +33 (0)3 20 43 65 91.
E-mail addresses: valerie.miri@univ-lille1.fr (V. Miri), nicolas.joly@univ-artois.fr (N. Joly).

0144-8617/$ – see front matter © 2010 Elsevier Ltd. All rights reserved.
doi:10.1016/j.carbpol.2010.10.045

and dispersion. According to Vaca-Garcia et al., each transition of fully substituted CEs obtained in a heterogeneous system occurred within a narrow temperature range, whatever the substituent chain length is. They explained this phenomenon by the formation of a crystalline phase of the fatty substituents between the cellulosic backbone (Vaca-Garcia, Gozzelino, Glasser, & Borredon, 2003).

The CEs under concern were obtained via an acylation pathway using pyridine in a heterogeneous medium. These reactions led to a non-homogeneous substitution only on the cellulosic particles surface.

Despite the substantial literature on cellulosic material research area, very few studies going from synthesis and chemical characterization to the physical and structural properties were carried out on the same material. This work deals with the analysis of CEs synthesized in a homogeneous system, and esterified uniformly onto the cellulose skeleton. Moreover, we are dealing here with a complete range of CEs esterified with fatty chains ranging from C8 to C18 with high DS values. The structural, thermal and thermomechanical analysis of cellulose esters were systematically performed using wide angle X-ray scattering (WAXS), differential scanning calorimetry, dynamic mechanical analysis (DMA) and uniaxial tensile tests respectively. The final goal of this investigation is to determine the structure–property relationships of CEs according to the substituted fatty chain length.

2. Experimental

2.1. Materials

All reagents were stored at room temperature and used without further purification: microcristalline cellulose (20 μm, Aldrich), whose degree of polymerization (DP = 150) was measured by a viscosimetric method using cupriethylenediamine and water as solvents (TAPPI Press, 1990); *N*,*N*-dimethyl-4-aminopyridine (DMAP, 99%, Acros); *N*,*N*-dimethylacetamide (DMAc, 99%, Acros); anhydrous lithium chloride (99%, Acros); octanoyl chloride (OcCl, 99%, Aldrich); decanoyl chloride (DCl, 98%, Aldrich); lauroyl chloride (LCl, 98%, Aldrich); myristoyl chloride (MCl, ≥99%, Fluka); palmitoyl chloride (PCl, 98%, Acros); stearoyl chloride (SCl, 90%, Fluka); chloroform (≥99%, Prolabo); methanol (≥99%, Prolabo). Deuterated chloroform was purchased from Aldrich and stored at 4 °C.

2.2. Acylation of cellulose by acyl chlorides

In a typical experiment, a 20 g L^{-1} cellulosic solution, consisting in pre-treated cellulose in a 6.7% LiCl/DMAc (v/w) system (Joly, Granet, & Krausz, 2003) (150 mL; 3 g; 18 mmol) and DMAP (6.6 g; 162 mmol; 3 equiv. per anhydroglucose unit) were stirred at 80 °C until complete solubilization. Fatty acyl chloride (5–8 equiv. per anhydroglucose unit according to fatty acid chloride) was then added. The mixture was heated classically at 80 °C during 3 h (Joly et al., 2006; Satgé, Verneuil, Branland, & Krausz, 2004; Vaca-Garcia, Thiebaud, Borredon, & Gozzelino, 1998). The product was precipitated by addition of methanol and the solid was purified by a repeated solubilization/precipitation process using chloroform and methanol, respectively, and finally dried in air at room temperature (Satgé et al., 2002) and the film was recovered by addition of water, after complete elimination of solvent. CEs were then converted into films via casting: CEs (10 g) were dissolved in 100 mL chloroform, filtered, and poured in a plate (20 cm × 20 cm). The solvent was then evaporated in air at room temperature, and the plastic was recovered by addition of water, after complete elimination of solvent (24 h).

All cast films were translucent and ductile, except for the one obtained from stearoyl chloride, which was extremely brittle so that no mechanical properties could be undertaken.

2.3. Chemical characterization

Every film has been characterized by Fourier transformed infra red (FTIR) spectroscopy using a Bruker Vector 22 FT-IR apparatus equipped with a diamond reflection accessory.

Nuclear magnetic resonance of proton (^{1}H NMR) spectroscopy was performed in $CDCl_3$ using a Bruker DRX-300 Spectrometer (operating at 300 MHz) to determine the degree of substitution (DS) by an integration method described elsewhere (Joly, Granet, Branland, Verneuil, & Krausz, 2005). The DS is defined as the number of fatty chains linked per anhydroglucose unit (maximum value of 3).

2.4. Structural characterizations

Wide angle X-ray scattering data were collected on a MAR345 Image plate detector, with Cu Kα radiation produced by a Bruker-Nonius FR591 rotating-anode generator equipped with an Osmic's confocal Max-flux optical system and running at 100 mA and 50 kV. Experiments were conducted at room temperature in the transmission mode on CE cast films.

2.5. Thermal behavior

DSC measurements were carried out on a Perkin-Elmer Diamond apparatus. The temperature and the heat flow scales were calibrated from the melting of high purity indium and zinc samples. About 10 mg of each CE film sample was used in the heating/cooling cycle experiments conducted at 20 °C min^{-1} under nitrogen atmosphere.

2.6. Dynamic mechanical analysis (DMA)

DMA measurements were performed on a Rheometrics RSA III apparatus operating in tensile mode at a frequency of 1 Hz in the temperature range $-120 < T < 110$ °C. Specimens with gauge width and length 5 mm × 24 mm were cut out from the CEs solvent-cast films. The temperature of T_β and T_α were taken at their respective tan δ peak maxima.

2.7. Uniaxial tensile behavior

Tensile testing was conducted on an Instron machine at room temperature, using specimens with L_0 = 24 mm and l_0 = 5 mm gauge length and width, respectively. The tensile tests were carried out at a constant crosshead speed of 1.44 mm min^{-1} which corresponds to an initial strain rate of 1×10^{-3} s^{-1}. The nominal stress σ and strain ε are defined conventionally as the ratio $F/(l_0 e_0)$ and $(L - L_0)/L_0$, respectively.

3. Results and discussion

In order to proceed to homogeneous cellulose modification as described in Scheme 1, it was necessary to dissolve cellulose. This polysaccharide is known to be insoluble in classical organic solvents and water. Nevertheless, particular solvent systems such as lithium chloride/*N*,*N*-dimethylacetamide (LiCl/DMAc) (Dawsey & McCormick, 1990), have to be used to dissolve this polysaccharide. This system of solvent (LiCl/DMAc) for cellulose solubilisation is really interesting since concentrated solutions of cellulose can be prepared without any degradation of the natural polymer in time (Dupont, 2003).

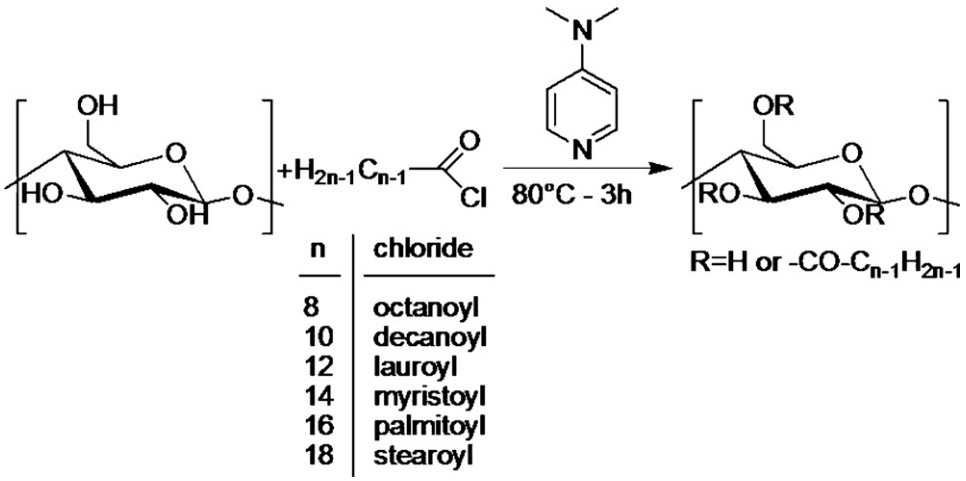

Scheme 1. Esterification of cellulose using acid chlorides.

Synthesis of plastic materials was performed by the internal plasticization of cellulose with fatty acids. These plastic films were obtained by cellulose acylation, using fatty chains with length ranging from octanoyl (C8) to stearoyl (C18), corresponding to the major fatty acids found in vegetal oil triglycerides. CEs were obtained by a method described elsewhere (Crépy et al., 2009; Joly et al., 2005), consisting in the reaction between fatty acid chlorides and cellulose, in presence of a basic catalyst, the *N*,*N*-dimethyl-4-aminopyridine (DMAP).

3.1. FTIR analysis

A comparison of the FTIR spectrum of native cellulose with cellulose laurate shows the relative efficiency of acylation (Fig. 1): a decrease in the intensity and a shift of the hydroxyl group characteristic band at 3400 cm^{-1} (–OH stretching) were observed (compared to the native cellulose spectrum). This difference indicates that a large amount of –OH groups were substituted. This phenomenon is linked with an increase in the intensity of the –C–H alkyl bonds characteristic signals at 2800–2900 cm^{-1} (–CH– antisymmetric and symmetric stretching of $–CH_2–$ and $–CH_3$), corresponding to the presence of fatty long chains. The concomitant appearance of two new bands is also observed; the first one at 1740 cm^{-1} (–C=O stretching), corresponding to the vibration of carbonyl ester groups, and the second one at 720 cm^{-1} characteristic for at least four linearly connected $–CH_2–$ groups ($–(CH_2)_4–$ rocking). That means fatty substituents have been linked directly onto cellulose. Same results are obtained whatever the substituent chain length is.

Table 1
^{1}H NMR chemical shifts of pure CEs and FAMEs (in $CDCl_3$).

δ (ppm)	Pure CEs	FAMEs (R–COO–CH_3)
H_{sugar}	5.50–3.00	–
$–CH_2–C=O$	2.34	2.34
$–CH_2–C–C=O$	1.60	1.60
$–(CH_2)_n–$	1.26	1.26
$–CH_3$	0.89	0.89
$–CO–O–CH_3$	–	3.68

3.2. ^{1}H NMR analysis

^{1}H NMR spectroscopy was used to estimate quantitatively the presence of the fatty chains on the cellulose backbone. Fig. 2 exhibits the ^{1}H NMR spectra for cellulose laurate. Note that spectra were similar for all CEs, irrespective of their fatty chain lengths. The acylation of cellulose was confirmed by integration of the characteristic signals of fatty acid protons from 0.89 to 2.34 ppm, and of the cellulosic backbone from 5.50 to 3.00 ppm (carbohydrate protons) in Table 1.

However, a new signal for CEs at about 3.68 ppm was sometimes observed (Fig. 2a). It appeared as a thin peak in the area of the H_{sugar} chemical shifts. We also noticed that this peak disappeared (Fig. 2b) after an additional purification step of the CEs plastic films (solubilization/precipitation process using chloroform and methanol respectively). This new peak corresponded to the ^{1}H NMR chemical shift of the ending methyl groups ($–CH_3$) of fatty acid methyl esters (FAMEs), which could be formed during the purification of CEs with methanol. In fact, during the first precipitation of the reaction medium with methanol, unreacted fatty acid chlorides reacted with methanol to form FAMEs and hydrochloric acid. A part of these

Table 2
Thermal transitions obtained by DSC.

CE materials	First heating				Second heating			
	T_{g1} (°C)	T_{g2} (°C)	T_m (°C)	ΔH_m (J/g)	T_{g2} (°C)	T_m (°C)	ΔH_m (J/g)	n_c
Octanoate: C8	–	93	58	–	75	–	–	–
Decanoate: C10	–	99	59	–	83	–	–	–
Laurate: C12	–	110	58	–	101	–	–	–
Myristate: C14	−20	110	49	8.3	102	3	27 (39)	2.67
Palmitate: C16	−4	122	43	18.7	114	23	44 (61)	4.84
Stearate: C18	6	–	44	50.2	–	40	55 (74.5)	6.67

–: not mesurable.
Between brackets, the melting enthalpy by weight of aliphatic chain.

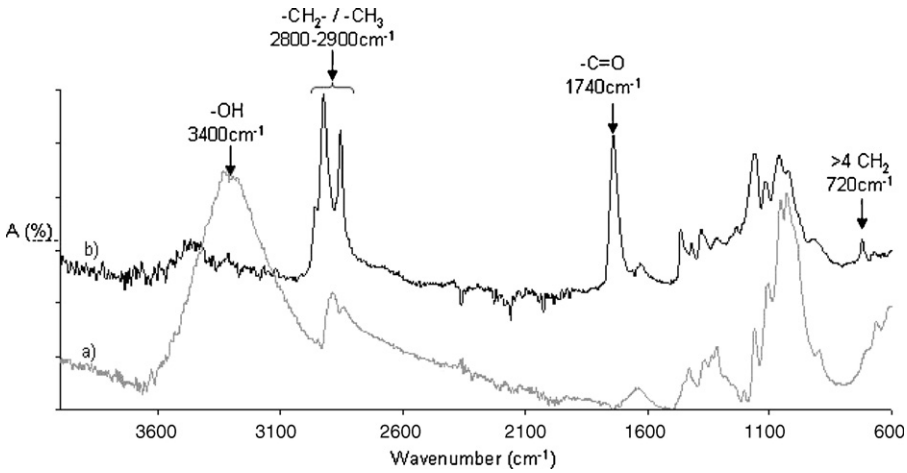

Fig. 1. FTIR spectra of a) native cellulose and b) cellulose laurate.

FAMEs can be retained inside the product. The longer the fatty substituent chains were, the more retained the FAMEs were. Hence, another purification step was needed. CEs were considered strictly as pure products when the chemical shift at 3.68 ppm disappeared.

The degree of substitution (DS) for all the derivatives was estimated to be 2.8 ± 0.1.

3.3. Thermal behavior

The thermograms recorded during the first heating reveal several thermal transitions for all the CEs: depending on the sample, one or two broad heat capacity jumps (glass transitions) and a broad endothermic peak (first order transition) were observed (Fig. 3a). The characteristic data for all these thermal transitions are reported in Table 2. The high temperature glass transition, T_{g2}, mainly related to the cellulosic backbone tends to increase with the fatty chain length. Similar trend has already been reported for comparable series of fully substituted *n*-alkyl esters of cellulose (Klarman, Galanti, & Sperling, 1969; Sealey et al., 1996). This result is indicative of an increased restriction in backbone cooperative motion as the alkyl chain length is increased beyond some critical value. For C14 to C18, a first order transition was clearly observed just above room temperature. This thermal transition is attributed to the melting of side chain crystals, as already observed for similar cellulose derivatives (Morooka et al., 1984; Sealey et al., 1996). As stated in literature, side chain crystallization can take place in polymers with rigid backbones and long *n*-alkyl side chains when its length exceeds 10 or 12 carbon atoms (Lee, Pearce, & Kwei, 1997a, 1997b; Sealey et al., 1996). In the present study, the thermograms of C8 to C12 recorded during the first heating exhibit a faint endotherm, suggesting the presence of small amount of crystals in the CEs with an alkyl side chain containing only 7 carbons. The area and broadness of the endothermic peak grow significantly as substituent chain lengthens, indicating an increase of crystallinity and a broad crystal thickness distribution respectively. The low temperature glass transition T_{g1}, rarely reported in papers dealing with cellulose derivatives, can be ascribed to the alkyl chain fraction which is not involved in the crystalline phase. In this case, the T_{g1} temperature shift with chain length may be related to the crystal content increase as shown below. Indeed, one may expect an

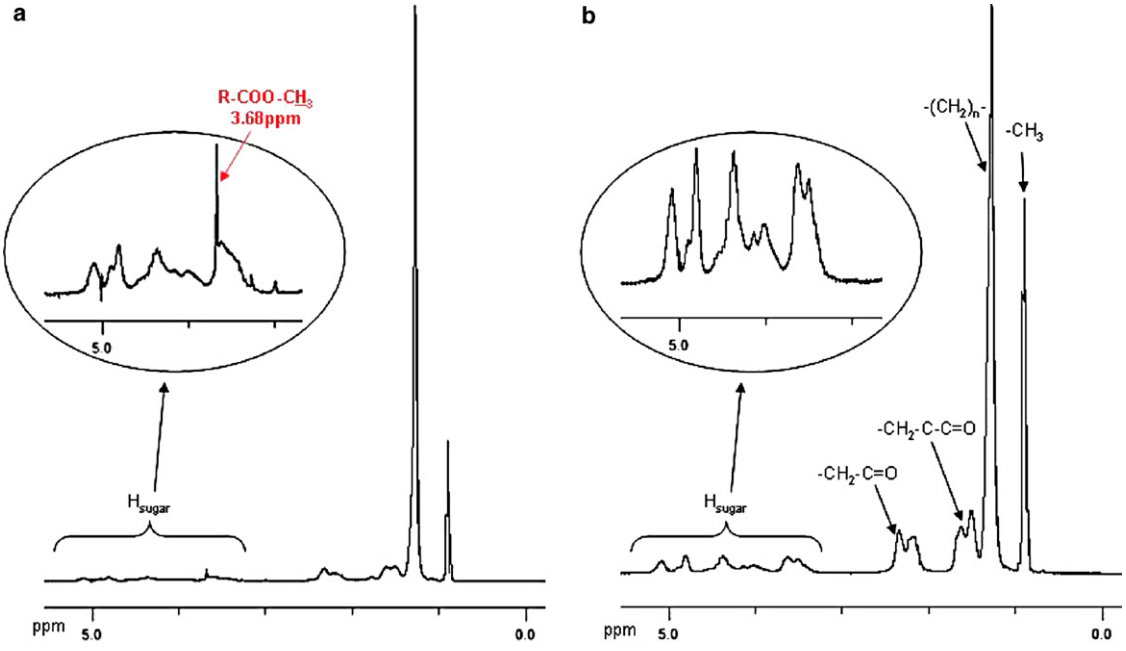

Fig. 2. ^{1}H NMR spectra of a) cellulose laurate polluted with FAME residues and b) pure cellulose laurate (in $CDCl_3$).

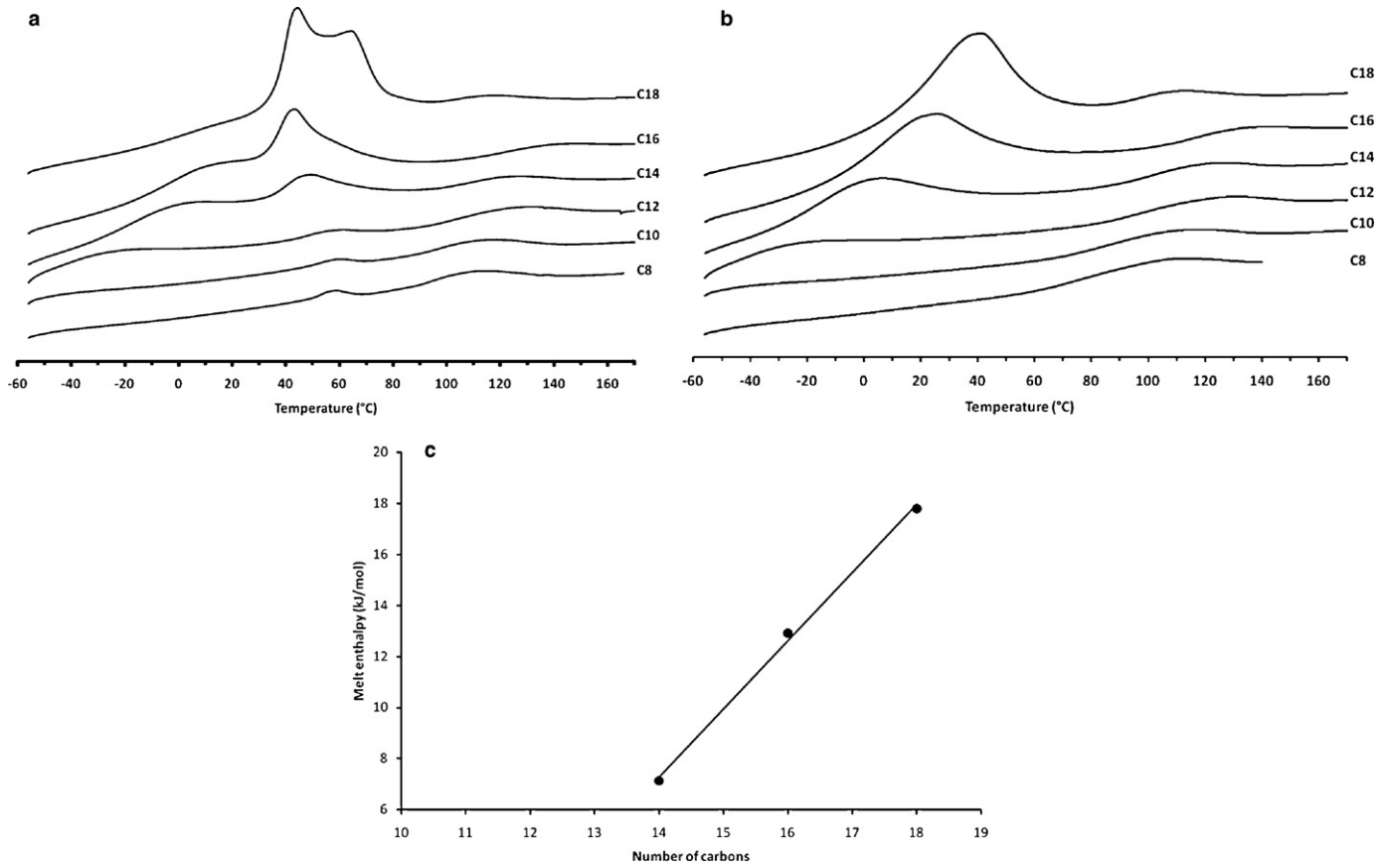

Fig. 3. a) First heating thermograms of the CEs cast films (endotherm up); (b) second heating thermograms of the CEs cast films; and c) enthalpies of fusion plotted as a function of carbon numbers of alkyl side chains.

increased constraint on the amorphous fraction of alkyl chains with the addition of crystals. One may notice that T_{g1} is not observed in the case of C8 and C10, because it occurs in a temperature range lower than $T = -60\,^{\circ}C$, as will be confirmed by DMA experiments described in the next section.

Besides, the thermograms recorded during the second heating (after a controlled cooling performed from 170 °C down to −60 °C at 20 °C min^{-1}) reveal an increase of the melting temperature with chain length, suggesting an increase in crystal thickness (Fig. 3b). Such a statement could not be made from the first heating scans since the different samples underwent different long-term annealing at 25 °C. The second heating scans related to the same thermal history were thus used to estimate the crystallinity of alkyl side chains in cellulose derivatives. Melting point and melt enthalpy for all systems are listed in Table 2. When the fusion enthalpies are plotted versus the number n of carbons in alkyl side chains, a linear correlation is found (Fig. 3c). This result has already been observed for various polymers having long alkyl side chains (Jordan, Feldeisen, & Wrigley, 1971; Lopez-Carrasquero et al., 2003; Shi et al., 2004). The slope of the solid line, k, which represents the contribution of each added methylene group to the enthalpy is sensitive to the type of crystal lattice adopted by the alkyl chains. In the present study, k is around 2.7 kJ mol^{-1} $CH_2{}^{-1}$ which is smaller than that of the corresponding n-alkanes (Lopez-Carrasquero et al., 2003; Shi et al., 2004). This indicates that the alkyl side chains form less-dense or less-ordered cells in the crystalline regions of CEs. However, the slope value is close to the one corresponding to the hexagonal lattice; suggesting that the alkyl side chains might be packed into a "hexagonal"-like crystal structure. This situation is similar to the one encountered for n-alkyl side chains in comb-like polymers (Lopez-Carrasquero et al., 2003; Shi et al., 2004). In addition, from Fig. 3c, a value of $n_0 \approx 11$ resulted for $\Delta H_m = 0$ kJ/mol for the series of these CEs which roughly represents the minimum length required for the side chain to be able to crystallize. According to Jordan (Jordan et al., 1971), the number of crystallized CH_2 groups in the side chain n_c may be estimated using the following relation: $n_c = \Delta Hm/k$. Results summarized in Table 2b show that only a part of the alkyl side chain participate in the crystallization and that the number of crystallized CH_2, n_c, increases with chain length.

3.4. Dynamic mechanical analysis (DMA)

The evolution of storage modulus E' and loss factor $\tan\delta$ as a function of temperature is presented in Fig. 4(a) and (b) respectively. For C14 and C16 samples, the DMA signal became erratic above room temperature, in relation to the melting of crystals, as evidenced from DSC experiments. All CEs exhibit a first relaxation below room temperature, revealed by a first drop in E' associated with a loss tangent peak. The temperature maximum for this relaxation increases with the ester substituent length (Table 3) except for the C8 and C10 samples which display similar relaxation temperature around −63 °C. These first relaxation temperatures are in good

Table 3
Temperatures of the mechanical relaxations measured in DMA.

CE materials	T_β (°C)	T_α (°C)
C8	−64	77
C10	−63	87
C12	−45	97
C14	−22	–
C16	−4	–

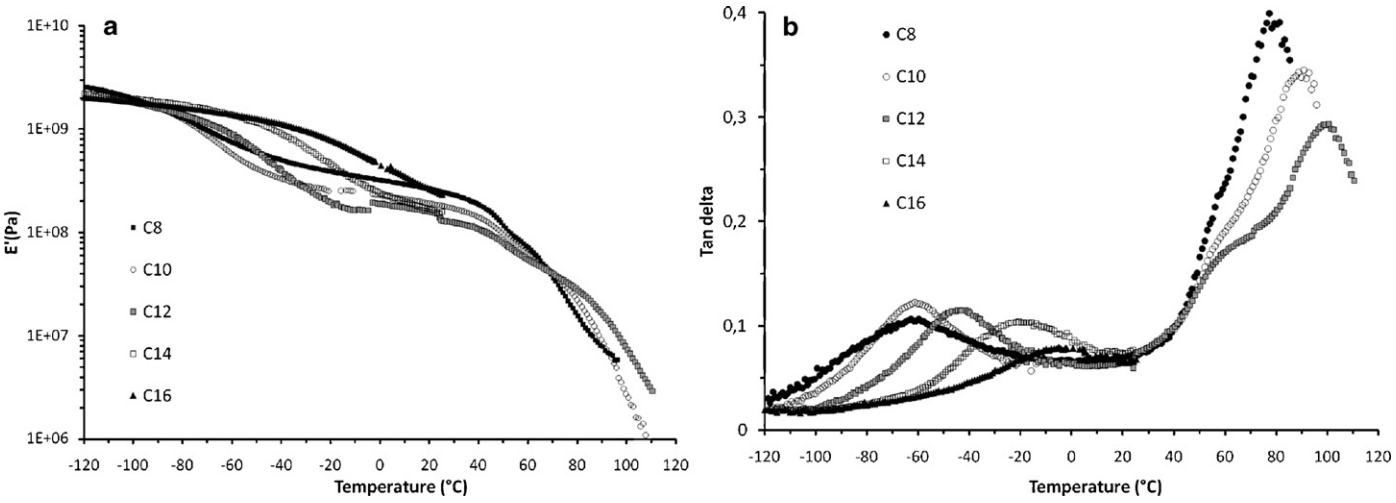

Fig. 4. Dynamic mechanical response of CE cast films as a function of temperature, recorded at 1 Hz frequency a) storage modulus E' and b) loss factor ($\tan\delta$).

agreement with the values of T_{g1} obtained by DSC recorded during the first heating. Additionally, DMA experiments clearly show the existence of a low temperature relaxation for C8 and C10.

Upon increasing temperature, an abrupt drop of E' accompanied by a broad loss tangent peak is observed for C8 to C12 samples. The shape of the loss tangent peaks suggests that two transitions overlap, the first one around 60 °C obviously independent of lateral chain length and a second one for which the peak temperature increases as the chain lengthens, located in the same temperature range as T_{g2}, observed in DSC experiments. Moreover, the $\tan\delta$ magnitude of both transitions, particularly the second one, seems to decrease as the chain length increases. Similar observations have already been reported in literature (Vaca-Garcia et al., 2003).

Only few studies report on a mechanical relaxation located around −60 °C for cellulose fatty esters. Morooka et al. assigned this relaxation to motions of the alkyl chains (Morooka, Norimoto, Yamada, & Shiraishi, 1983). The drop of E' suggests that this relaxation may be assigned to cooperative motions of the non crystallized part of the lateral chains. The temperature increase of this relaxation peak with the chain length may result from the crystallization of a part of the aliphatic chain as revealed by DSC experiments. It is expected that crystallization should hinder the mobility of the rest of the lateral chain. Note that Vaca-Garcia et al. who studied homologous series of fully substituted *n*-alkyl esters of cellulose have not observed any relaxation in this temperature range probably because samples are heated at 110 °C prior to analysis (i.e. in a situation similar to the 2nd heating of DSC experiments for which no heat capacity jump was observed around −60 °C). The transition around 60 °C which seems fairly constant in cellulose triesters whatever the size of the lateral chains is, depends on the degree of substitution. The temperature maximum of this transition decreases as the side chain length increases for partially substituted CE (Vaca-Garcia et al., 2003). Several assignments have been proposed to explain the molecular origin of this relaxation such as a boat-chair configuration change of the glucose ring (Klarman et al., 1969), motion of oxycarbonyl group of the side chain (Ogura, Miyachi, Sobue, & Nakamura, 1975) or local motion of the aliphatic substituents. From the present study, it is difficult to assign the specific group implied in this mechanical relaxation. However, it may be already assumed that this relaxation is rather due to the glucose ring and/or the oxycarbonyl group, considering that mobilities of amorphous alkyl chain are already unlocked at lower temperature. Solid state ^{13}C NMR experiments might clarify the molecular origin of the relaxation. The higher temperature relaxation is attributed to cooperative motions in the cellulose backbone. The temperature increase of this main relaxation as the lateral chain lengthens indicates that mobility in the cellulose backbone is increasingly restricted when the substituent chain is long enough.

3.5. Structural characterization

Fig. 5a shows the X-ray diffraction profiles of all film samples. All diffractograms display a major reflection in the low angle region ($1° < 2\theta < 4°$) and a broad and weak halo in the region $2\theta = 16–24°$. In the case of C14, C16 and C18, a weak additional diffraction in the region $2\theta = 5–7°$ is also noticed, which may be attributed to the third order of the small angle peak. The location of these reflections changes as a function of the fatty chain length. The *d* spacings of the corresponding diffraction peaks of each sample are summarized in Table 4.

Regarding the small angle reflections, the corresponding intermolecular distance increases steadily with the number of carbon atoms in the side chain, as shown in Fig. 5b. This indicates that these materials organize in a layered type structure, as already reported for similar CEs (Arici, Greiner, Hou, Reuning, & Wendorff, 2000; Lee, Pearce, & Kwei, 1998). It is difficult to propose an exact structural description of the packing of the chain molecules from these X-ray diffractograms. However, a structural model in fair agreement with the results obtained so far may be suggested. The simplest structural representation would involve a layered structure composed of a planar arrangement of parallel cellulosic backbones with fully extended flexible side chains oriented perpendicular to the planar structure (Scheme 2). In order to evaluate the relevance of this structural model, the layer spacing may be estimated as a function of number of carbon atoms, taking into account only the aliphatic part of the side chain assuming no interdigitation of the side chains. The result of this computation corresponds to the dotted line in Fig. 5b. Comparison of data with this crude estimate as a function of number of carbons in the range from 7 to 15 reveals that the

Table 4
WAXS diffractions (Å) of the CE cast films.

CE materials	Low-angle region		Wide-angle region
C8	21.2	ND	4.5
C10	26.1	ND	4.5
C12	28.8	ND	4.5
C14	37.1	13.0	4.4
C16	41.8	14.9	4.3
C18	ND	16.8	4.2

ND: not detected.

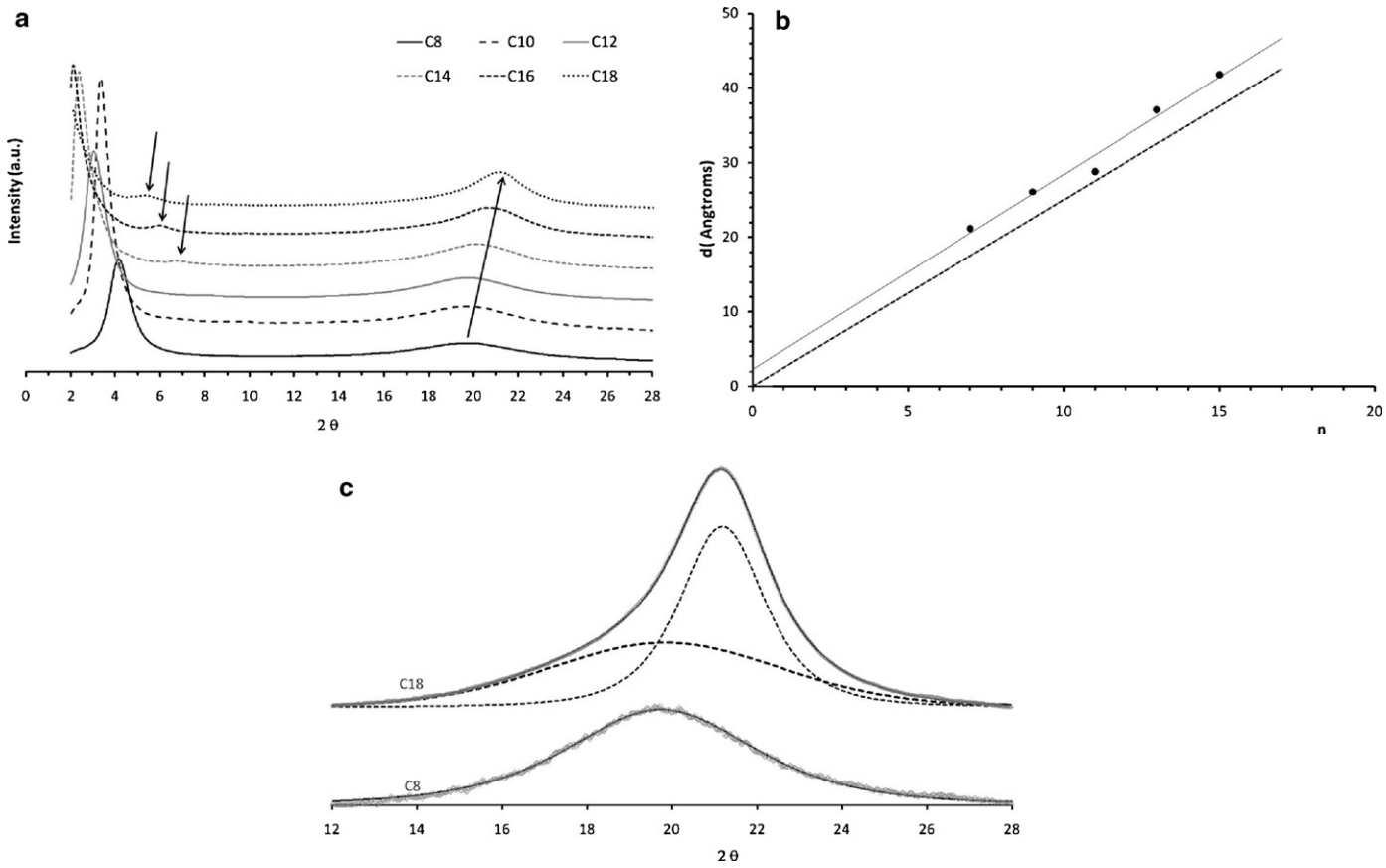

Fig. 5. a) X-ray diffractograms of the CE cast films; b) variation of the layer distance as a function of *n*, the number of carbons in the aliphatic side chain (slope = 2.61 Å per carbon); c) deconvoluted peaks superimposed on the experimental curves for C8 and C18 cellulosic esters.

slopes remain similar. This is indicative of the fact that no drastic change in the structural organization occurs as the alkyl chain length is increased, i.e. no major evolution implying tilt and interdigitation is taking place, which would result in a leveling off of the *d*–*n* plot of Fig. 5b.

Lateral chain order is suggested in the wide angle region of the diffractograms as indicated by the decrease of the peak width in the region $2\theta = 16–24^{\circ}$ as side chain length is increased. To elucidate the structural evolution, a deconvolution of the $I(2\theta)$ profiles was attempted using Peakfit software. Contributions of the amorphous and crystalline phases were approximated by Pearson VII functions.

Deconvoluted peaks are superimposed on the experimental curves for C8 and C18 in Fig. 5c and the results from profile analysis of the two scans are summarized in Table 5. The $I(2\theta)$ profile of

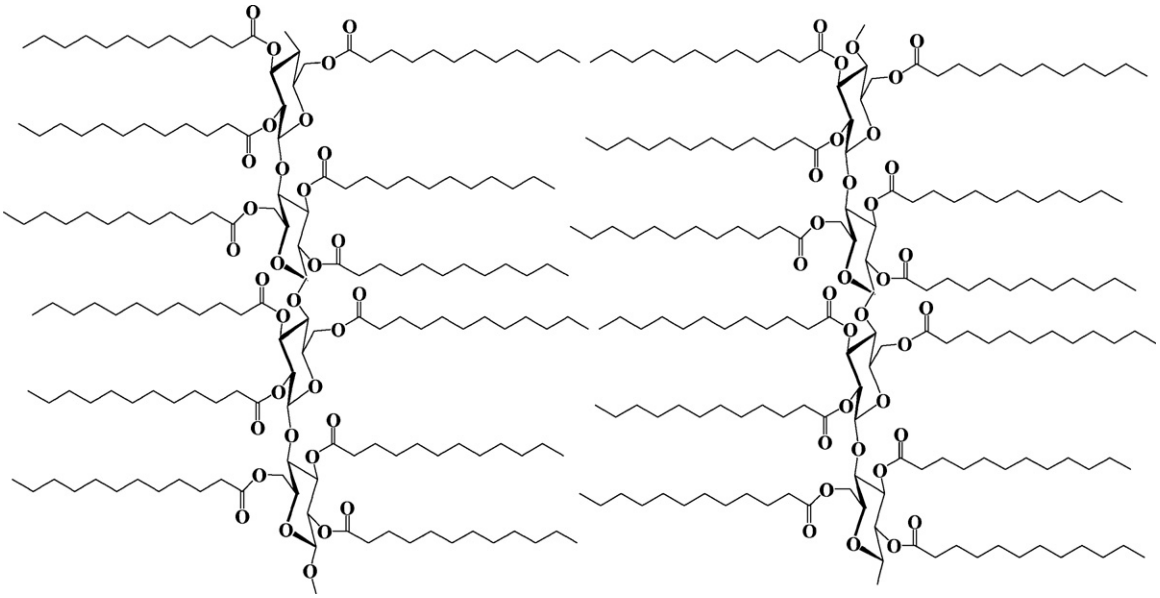

Scheme 2. Possible representation of a structural model for cellulosic laurate cast films.

Table 5
X-ray scattering parameters.

CE materials	Amorphous	"Crystalline"
C8		
2θ	19.7	–
FWHM	5.3	–
C18		
2θ	19.8	21.2
FWHM	6.4	2.4

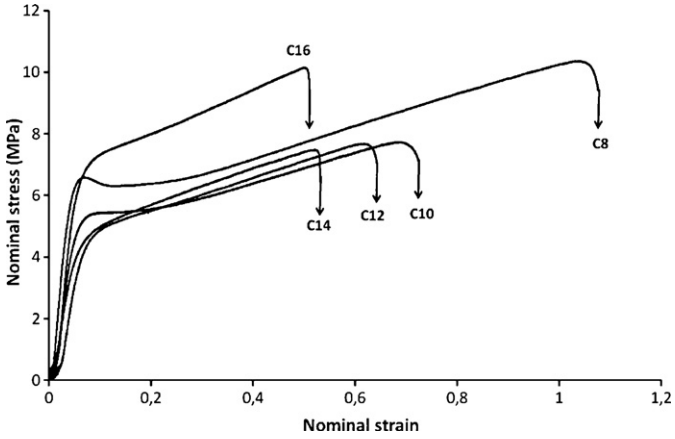

Fig. 6. Nominal stress–strain curves of the CE cast films under uniaxial drawing at $T = 20\,^{\circ}C$.

C8 can be fitted by one Pearson function characterized by a significant full-width at half-maximum (FWHM) indicative of a material in mainly disordered state. Two Pearson functions are needed for C18: one of them, much akin to the function used for C8 with similar maximum peak position and broad FWHM; the second Pearson function is characterized by a "narrower" FWHM indicating that this peak is rather relevant to a more ordered structure. These findings are in good agreement with the DSC experiments which have clearly shown the presence of crystals in C18. In addition, based on n-paraffin crystal structures (reference), the maximum peak position of the second Pearson function in the case of C18 located at 4.2 Å suggests that the aliphatic side chains are rather arranged into a α-hexagonal lattice, in agreement with the previous interpretation of DSC results. Moreover, this result is in good agreement with investigations on poly(*n*-alkyl methacrylates) and poly(*n*-alkyl itaconate)s which have shown that the alkyl side chains are able to crystallize into hexagonal packing (Lopez-Carrasquero et al., 2003).

3.6. Uniaxial tensile behavior

Fig. 6 displays the stress–strain behavior of solvent-cast films at room temperature. All samples exhibit a rather ductile behavior except for the C18 material which is extremely brittle, as mentioned previously. These preliminary results show that as the lateral chain length is increased, the strain at break tends to drop whereas no clear evolution of the yield stress is evidenced (Table 6). The next step will focus on a detailed investigation of the structural evolution of sample organization upon drawing, in relation to the key molecular parameters of chain substitution and thermo-mechanical history.

Table 6
Yield stress, σ_y and strain at break, ε_{break}, of CE cast films at $T = 23\,^{\circ}C$.

CE materials	σ_y (MPa)	ε_{break}
C8	6.40 ± 0.01	1.0 ± 0.1
C10	5.25 ± 0.24	0.7 ± 0.2
C12	4.84 ± 0.09	0.6 ± 0.2
C14	4.80 ± 0.14	0.5 ± 0.1
C16	7.06 ± 0.01	0.4 ± 0.2

4. Conclusion

Fully substituted cellulose fatty ester derivatives were synthesized in homogeneous medium, and then converted into films by casting. All of the structural, thermal and mechanical properties were performed onto these samples, to determine the relationships of these properties with the side chain length. Thermal analysis experiments had revealed the presence of two glass transition temperatures, which increase with alkyl chain length: a high glass transition temperature (between 70 °C and 115 °C) related to the cellulosic backbone and a low one (from −64 °C to 6 °C) rather attributed to alkyl chains which were not involved in crystalline phase. A melting point had also been observed (4–50 °C) for these cellulosic films, whose temperature increases with the fatty chain length. DSC and X-ray data indicate that alkyl side chains with more than 11 carbons were able to crystallize in hexagonal lattice. Moreover, a structural model was proposed in which the cellulosic backbones display a planar organization, together with an arrangement of the alkyl side chains perpendicular to the cellulose backbone without interdigitation. Finally, regarding the tensile deformation behavior, the strain at break decreases significantly whereas no clear evolution of the yield stress was observed as a function of fatty chain lengths.

References

Arici, E., Greiner, A., Hou, H., Reuning, A., & Wendorff, J. H. (2000). Optical properties of guest host systems based on cellulose derivatives. *Macromolecular Chemistry and Physics*, *201*, 2083–2090.
Chauvelon, G., Gergaud, N., Saulnier, L., Lourdin, D., Buléon, A., Thibault, J. F., et al. (2000). Esterification of cellulose-enriched agricultural by-products and characterization of mechanical properties of cellulosic films carbohydrate. *Carbohydrate Polymers*, *42*, 385–392.
Crépy, L., Chaveriat, L., Banoub, J., Martin, P., & Joly, N. (2009). Synthesis of cellulose fatty esters as plastics – influence of the degree of substitution and the fatty chain length on mechanical properties. *ChemSusChem*, *2*, 165–170.
Dawsey, T. F., & McCormick, C. L. (1990). The lithium chloride/dimethylacetamide solvent for cellulose: A literature review. *Journal of Macromolar Science Reviews Macromolar Chemistry and Physics*, *30*, 405–440.
Dupont, A. L. (2003). Cellulose in lithium chloride/N N-dimethylacetamide, optimisation of a dissolution method using paper substrates and stability of the solutions. *Polymer*, *44*, 4117–4126.
Edgar, K. J., Buchanan, C. M., Debenham, J. S., Rundquist, P. A., Seiler, B. D., Shelton, M. S., et al. (2001). Advances in cellulose ester performance and application. *Progress in Polymer Science*, *26*, 1605–1688.
Heinze, T., & Liebert, T. (2001). Unconventional methods in cellulose functionalization. *Progress in Polymer Science*, *26*, 1689–1762.
Joly, N., Granet, R., Branland, P., Verneuil, B., & Krausz, P. (2005). New methods for acylation of pure and sawdust – extracted cellulose by fatty acid derivates – thermal and mechanical analyses of cellulose-based plastic films. *Journal of Applied Polymer Science*, *97*, 1266–1278.
Joly, N., Granet, R., & Krausz, P. (2003). Crosslinking of cellulose by olefin metathesis. *Journal of Carbohydrate Chemistry*, *22*, 47–55.
Joly, N., Martin, P., Liénard, L., Rutot, D., Stassin, F., Granet, R., et al. (2006). Effect of degree of substitution on the mechanical and thermomechanical properties of lauroyl cellulose ester films. *E-Polymers*, *70*, 1–9.
Jordan, E. F., Feldeisen, D. W., & Wrigley, A. N. (1971). Side-chain crystallinity. I. Heats of fusion and melting transitions on selected homopolymers having long side chains. *Journal of Polymer Science*, *9*, 1835–1852.
Klarman, A. F., Galanti, A. V., & Sperling, L. H. (1969). Transition temperatures and structural correlations for cellulose triesters. *Journal of Polymer Science*, *7*, 1513–1523.
Lee, J. L., Pearce, E. M., & Kwei, T. K. (1997a). Side-chain crystallization in alkyl-substituted semiflexible polymers. *Macromolecules*, *30*, 6877–6883.
Lee, J. L., Pearce, E. M., & Kwei, T. K. (1997b). Morphological development in alkyl-substituted semiflexible polymers. *Macromolecules*, *30*, 8233–8244.
Lee, J. L., Pearce, E. M., & Kwei, T. K. (1998). Liquid crystallinity and side chain order in partially substituted semi-flexible polymers. *Macromolecular Chemistry and Physics*, *199*, 1003–1011.
Lopez-Carrasquero, F., Martinez de Ilarduya, A., Cardenas, M., Carillo, M., Arnal, M. L., Laredo, E., et al. (2003). New comb-like poly(n-alkyl itaconates with crystallizable side chains. *Polymer*, *44*, 4969–4979.

Malm, C., Mench, J., Kendall, D., & Hiatt, G. (1951). Aliphatic acid esters of cellulose. Preparation by acid chloride–pyridine procedure. *Industrial & Engineering Chemistry*, *43*, 684–688.

Mohanty, A. R., Wibowo, H., Misra, M., & Drzal, L. T. (2003). Development of renewable resource based cellulose acetate bioplastic: Effect of process engineering on the performance of cellulosic plastic. *Polymer Engineering & Science*, *43*, 1151–1161.

Morooka, T., Norimoto, M., Yamada, T., & Shiraishi, N. (1983). Viscoelastic properties of cellulose acylates. *Wood Research*, *69*, 61–71.

Morooka, T., Norimoto, M., Yamada, T., & Shiraishi, N. (1984). Dielectric properties of cellulose acylates. *Journal of Applied Polymer Science*, *29*, 3981–3990.

Nagatani, A., Endo, T., Hirotsu, T., & Furukawa, M. (2005). Preparation and properties of cellulose–olefinic thermoplastic elastomer composites. *Journal of Applied Polymer Science*, *95*, 144–148.

Ogura, K., Miyachi, Y., Sobue, H., & Nakamura, S. (1975). Infrared spectroscopic studies of polymer transitions. 4. Second-order transition of cellulose triacetate in the vicinity of 30 °C. *Die Makromoleculare Chemie*, *176*, 1173–1178.

Satgé, C., Verneuil, B., Branland, P., Granet, R., Krausz, P., Rozier, J., et al. (2002). Rapid homogeneous esterification of cellulose induced by microwave irradiation. *Carbohydrate Polymers*, *49*, 373–376.

Satgé, C., Verneuil, B., Branland, P., & Krausz, P. (2004). Synthesis and properties of biodegradable plastic films obtained by microwave-assisted cellulose acylation in homogeneous phase. *Comptes Rendus Chimie*, *7*, 135–142.

Sealey, J. E., Samaranayake, G., Todd, J. G., & Glasser, W. G. (1996). Novel cellulose derivatives. IV. Preparation and thermal analysis of waxy esters of cellulose. *Journal of Polymer Science: Part B: Polymer Physics*, *34*, 1613–1620.

Shi, H., Zhao, Y., Zhang, X., Jiang, S., Wang, D., Han, C. C., et al. (2004). Phase transition and conformational variation of N-alkylated branched poly(ethyleneimine) comblike polymer. *Macromolecules*, *37*, 9933–9940.

TAPPI Press-Viscosity of pulp (capillary viscosimeter method). (1990). TAPPI test methods 1991. Atlanta: Tappi Press. 1, Ref. T230 om-89.

Thiebaud, S., Borredon, M. E., Baziard, G., & Senocq, F. (1997). Properties of wood esterified by fatty-acid chlorides. *Bioresource Technology*, *59*, 103–107.

Vaca-Garcia, C., Gozzelino, G., Glasser, W. G., & Borredon, M. E. (2003). Dynamic mechanical thermal analysis transitions of partially and fully substituted cellulose fatty esters. *Journal of Polymer Science: Part B: Polymer Physics*, *41*, 281–288.

Vaca-Garcia, C., Thiebaud, S., Borredon, M. E., & Gozzelino, G. (1998). Cellulose esterification with fatty acids and acetic anhydride in lithium chloride/N,N-dimethylacetamide medium. *Journal of the American Oil Chemists' Society*, *75*, 315–319.